THE JOURNAL OF BIOLOGICAL CHEMISTRY
Vol. 279, No. 24, Issue of June 11, pp. 25359–25363, 2004
Printed in U.S.A.

Three-dimensional Reconstruction of *Agrobacterium* VirE2 Protein with Single-stranded DNA*

Received for publication, February 18, 2004, and in revised form, March 29, 2004
Published, JBC Papers in Press, March 30, 2004, DOI 10.1074/jbc.M401804200

Asmahan Abu-Arish‡, Daphna Frenkiel-Krispin‡, Tobin Fricke‡, Tzvi Tzfira§, Vitaly Citovsky§, Sharon Grayer Wolf¶, and Michael Elbaum‡‖

From the ‡Department of Materials and Interfaces and ¶Electron Microscopy Unit, Weizmann Institute of Science, Rehovot 76100, Israel and §Department of Biochemistry and Cell Biology, State University of New York, Stony Brook, New York 11794-5215

Agrobacterium tumefaciens **infects plant cells by a unique mechanism involving an interkingdom genetic transfer. A single-stranded DNA substrate is transported across the two cell walls along with the bacterial virulence proteins VirD2 and VirE2. A single VirD2 molecule covalently binds to the 5′-end of the single-stranded DNA, while the VirE2 protein binds stoichiometrically along the length of the DNA, without sequence specificity. An earlier transmission/scanning transmission electron microscopy study indicated a solenoidal ("telephone coil") organization of the VirE2-DNA complex. Here we report a three-dimensional reconstruction of this complex using electron microscopy and single-particle image-processing methods. We find a hollow helical structure of 15.7-nm outer diameter, with a helical rise of 51.5 nm and 4.25 VirE2 proteins/turn. The inner face of the protein units contains a continuous wall and an inward protruding shelf. These structures appear to accommodate the DNA binding. Such a quaternary arrangement naturally sequesters the DNA from cytoplasmic nucleases and suggests a mechanism for its nuclear import by decoration with host cell factors. Coexisting with the helices, we also found VirE2 tetrameric ring structures. A two-dimensional average of the latter confirms the major features of the three-dimensional reconstruction.**

Agrobacterium tumefaciens is the causative agent of the crown gall disease in many plant species (1, 2). To attack its host, *Agrobacterium* employs a unique and complex transformation process. Genetic material is transported from the bacterium into the host cell and then into the nucleus, where it integrates stably to the host genome (for review, see Refs. 3–7). Expression of the genes encoded by the invading DNA leads to cell proliferation and to gall formation. Within this tumor-like tissue, genes are expressed for enzymes that govern production of opine compounds, amino acid derivatives utilized exclusively by the *Agrobacterium* (8). In nature its host range is limited mainly to dicotyledonous plants (1). Under controlled culture conditions, on the other hand, *Agrobacterium* has been shown to possess a broad range of hosts, including monocots (*e.g.* see Ref. 9), yeast (10), fungi (11, 12), and even human tissue cells (13).

The molecular basis for the genetic transformation process is the transfer of a well defined single-stranded DNA fragment, the tDNA, from the *Agrobacterium* tumor-inducing plasmid to the host cell nucleus. The process is mediated by a set of chromosomal (*chv*) and tumor-inducing plasmid-encoded virulence (*vir*) genes (for review, see Refs. 3–7), as well as by specific host factors (for review, see Refs. 4, 6, and 7). The tDNA itself does not carry any signals for its processing, transport, nuclear import, and integration; the only *cis* elements that define the tDNA region are specific 25-bp direct repeats at its left and right borders (14, 15). For this reason primarily, tDNA transfer is not sequence-dependent, leading to the emergence of *Agrobacterium* as a powerful tool for modifications of plants both in the laboratory and in molecular plant breeding (16–18).

Upon induction of the *vir* region by detection of plant-specific wound signals, the VirD1-VirD2 bacterial protein complex nicks both borders on the non-coding strand of the tDNA region and releases a single-stranded tDNA molecule (the T-strand). A single VirD2 molecule remains attached to the T-strand 5′-end (19, 20), while the remaining oligonucleotide is covered stoichiometrically with VirE2 molecules (21–23). It remains a matter of debate whether the T-strand is exported fully assembled with VirE2 (23) or whether the formation of a mature T-complex occurs only within the host cell cytoplasm (24, 25). In one model, the T-complex is exported to the host cell cytoplasm through a *virB*/*virD4*-encoded channel (26, 27). Alternatively, the T-strand-VirD2 complex and the VirE2 molecules may be exported from the *Agrobacterium* independently and meet only later in the host cytoplasm, where they assemble into a mature T-complex. The T-complex is then imported into the host cell nucleus, where it may be expressed transiently or integrated into the host genome, thus finalizing the transformation process.

Both VirD2 and VirE2 play crucial roles in tDNA nuclear import and integration. VirD2 promotes nuclear import through its interaction with a host karyopherin α receptor (28). It also appears to be involved in intranuclear transport and in tDNA integration (29–32). Association of VirE2 with the T-strand is required for protection from exonucleolytic degradation (22), as well as for nuclear import via interaction with the intermediary host factor VIP1 (33). There appears to be some redundancy in the functions. For very short tDNAs, VirE2 may be replaced by other single-strand binding proteins without inhibiting nuclear import (34), while in other cases VirE2 alone can mediate import of tDNA in the absence of VirD2 (35). VirE2 has also been reported to form membrane channels *in vitro* (36), suggesting that such channels might be involved in as-

* This work was supported in part by the Minerva Research Foundation, which is funded through the German Federal Ministry for Education and Research (BMBF), by the United States-Israel Binational Agricultural Research and Development Fund, by the Gerhardt M. J. Schmidt Center for Supramolecular Architecture, and by the Jean and Jula Goldwurm Foundation. The costs of publication of this article were defrayed in part by the payment of page charges. This article must therefore be hereby marked "*advertisement*" in accordance with 18 U.S.C. Section 1734 solely to indicate this fact.

‖ To whom correspondence should be addressed. Tel.: 972-8-9343537; Fax: 972-8-9344138; E-mail: michael.elbaum@weizmann.ac.il.

sisting the passage of DNA through the plant plasma membrane (37).

There are virtually no length limitations for the tDNA sequences, and *Agrobacterium* has been shown to be capable of transporting and integrating tDNAs up to 150 kb long (38, 39). Extra copies of the *virE2* loci were required for efficient transport of such large molecules, further supporting the role of VirE2 as an essential chaperone of the T-complex (39). A prior study has shown that the cooperative binding of VirE2 to single-stranded DNA shapes the T-complex into a regular solenoid (or telephone coil) shape, and the study used scanning transmission electron microscopy to establish basic structural and stoichiometric parameters (40). Resolution at a molecular level was not available, however.

In this work we report a three-dimensional reconstruction of the VirE2-ssDNA[1] complex using electron microscopy and image-processing techniques. The helical T-complex structure is found to form a hollow solenoid shape, with a putative ssDNA binding site near the inner diameter of the structure. This structure appears to satisfy several functional needs for nuclear import; the ssDNA is physically shielded from nucleases during the transfer process, and the solenoid winding results in a 7-fold foreshortening of the ssDNA length, facilitating its transport through both the cytoplasm and the nuclear pore. An independent corroboration of the three-dimensional reconstruction was provided from the analysis of tetrameric structures often found adjacent to the helical complexes.

EXPERIMENTAL PROCEDURES

Sample Preparation and Image Acquisition—Nopaline strain VirE2 was expressed and purified from inclusion bodies in *Escherichia coli* as described by Citovsky *et al.* (22). M13 single-strand DNA was purchased from New England Biolabs.

For the three-dimensional reconstruction, a scan of conditions was performed to optimize regularity and length of the helices. M13 DNA was first heated to 65 °C and then cooled rapidly on ice and mixed, at room temperature, with purified VirE2 in 6-μl aliquots at a protein:DNA ratio of 1:1 by weight (80 μg/ml DNA). The mixture was left for 24 h to form and anneal. For the tetramer study, the protein:DNA ratio was increased to 3:1, and incubation was performed overnight at room temperature. Samples were deposited onto freshly glow-discharged carbon-coated grids, negatively stained in 1.5% uranyl acetate, and air-dried.

Images were recorded in an FEI Tecnai F20FEG transmission electron microscope equipped with a 1k $\times$ 1k Teitz charge-coupled device camera in 2 $\times$ 2 tiling mode at a scale of 0.32 nm/pixel. Magnification of the microscope was verified using tobacco mosaic virus.

A series of 50 CCD images were collected at various defocus values ranging from 0.6 to 2.7 μm, with first zeros in the contrast transfer function (CTF) ranging from 1.2 to 2.6 nm. The CTFs were corrected by phase flipping using the BSoft package (41).

Image Processing—Image processing for three-dimensional reconstruction used the iterative helical real space reconstruction (IHRSR) method (42) with minor modifications as follows. Particles were picked using a program written in-house (available on request) for selecting filaments. Lines are drawn over the filaments using the computer mouse, and the program selects coordinates for boxing the particles at a user-selected interval while keeping track of groups of particles coming from the same filament. This is useful where polarity can be determined per filament by two-dimensional averaging. The program also keeps track of the angle of the overlaid, user-drawn line, which is used for preliminary vertical orientation of the particles. 8440 particles of 80 $\times$ 80 pixel size were selected from the filaments.

Visual inspection showed that despite efforts to avoid bad regions, the semiautomated particle picking included a large fraction of images containing breaks, kinks, or obvious staining artifacts. To select the good particles, a classification was performed using the self-organizing map (SOM) algorithms of the XMIPP package (43). The entire set was first low pass-filtered to 3.2 nm, and a reference-free alignment was performed using the Spider software package (44). Transformations in x, y, and in-plane angle θ were imposed, and the data set was fed to the kernel density SOM procedure using a 10 $\times$ 10 grid. The procedure generates a grid of code vectors that represent the assigned images. It was verified that clean looking code vectors represented classes of clean particles, while particles assigned to defect-ridden code vectors were themselves of poor quality. The procedure was repeated several times with different parameters, and in each case a set of roughly 3000 good particles was obtained. Further processing was conducted on a set containing 2943 particles.

The IHRSR method assigns azimuthal angles to images by cross-correlation with projections of an initial model volume. The images are then back-projected according to that assignment list to produce a new volume. This is searched for a minimal residual over a grid of helical symmetries (rise and units/turn). The symmetry corresponding to the minimal residual is imposed, and the resulting symmetrized volume becomes the new starting model.

The initial model was an unstructured helix of 5.2-nm pitch and 15.4-nm diameter. The following minor modifications were made in the procedure. At the end of each cycle the parameters of symmetrization were randomized slightly away from the minimal residual condition, by an amount up to one step in the grid search, so as to avoid trapping in local minima. To speed convergence (and gain confidence in the direction of the reconstruction) the cross-correlations were performed in a series of progressively increasing (*i.e.* improving) resolution shells by low pass filtering the projections of the model in a programmed manner: 12 cycles at 3.2 nm, 12 cycles at 2.8 nm, 6 cycles at 2.4 nm, and 6 cycles at 2.0 nm. Intermediate stages of convergence could be seen in the helical symmetries and by inspection of isosurface contours of the reconstructed volume. A uniform distribution of the angular reference assignments was also confirmed at each stage. The symmetry refinement was stopped at a resolution cutoff of 2.0 nm; for higher resolutions the angular assignments became unstable. The density maps presented are also cut off at 2.0 nm, although the ultimate resolution of the reconstruction should be somewhat better than that of the alignment criteria.

Additionally, a crude tomographic reconstruction was carried out to confirm that the hollow structures did not collapse in the staining and drying processes.

Rings were selected from CCD images by hand, using the EMAN Boxer program (45), yielding a data set of 1084 particles. A low pass filter at 2.0 nm was applied within the first zero of the CTF at the relevant defocus. Reference-free alignment was then performed using Spider software (44), yielding a two-dimensional average. Images, isocontours, and isosurfaces were prepared for figures using Amira (www.amiravis.com).

RESULTS

A typical view of the complex of VirE2 protein with single-stranded DNA (circular ssDNA from M13) is shown in Fig. 1*A*. We scanned sample preparation conditions to optimize length and regularity of the helices. We found that due to strongly cooperative binding (22), we could inhibit nucleation but still achieve complete coverage by using a strongly substoichiometric ratio of protein to DNA and a long incubation time. Regular helices can be analyzed by classical Fourier-Bessel methods (46). Despite our efforts, however, the structure was often broken by abrupt kinks or gaps, in which the progression of the helical phase was lost. Therefore we applied the recently developed IHRSR method (42). In this analysis, short helical segments boxed from the original images are treated as single particles and are reconstructed using multireference-based image cross-correlation methods with no symmetry imposed. A search for helical symmetry (axial rise and angular turn/subunit) is carried out and imposed on the reconstructed three-dimensional model, which then serves as a reference for the next iteration. This process is iterated until a stable reconstruction is achieved. The established method and slight modifications to it are described in more detail under "Experimental Procedures."

Individual helical segments were boxed from the original images and classified to form a data set containing helical particles with minimal defects as described under "Experimen-

[1] The abbreviations used are: ssDNA, single-stranded DNA; CTF, contrast transfer function; IHRSR, iterative helical real space reconstruction; SOM, self-organizing map.

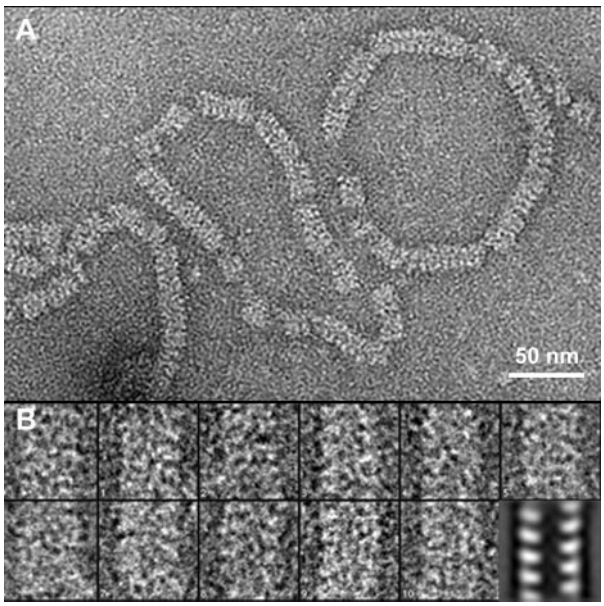

FIG. 1. *A*, the complex of VirE2 protein with single-strand DNA is observed in transmission electron microscopy. *B*, gallery of raw particles aligned by reference-free procedure. The *rightmost panel* shows the average of the 2943 aligned particles.

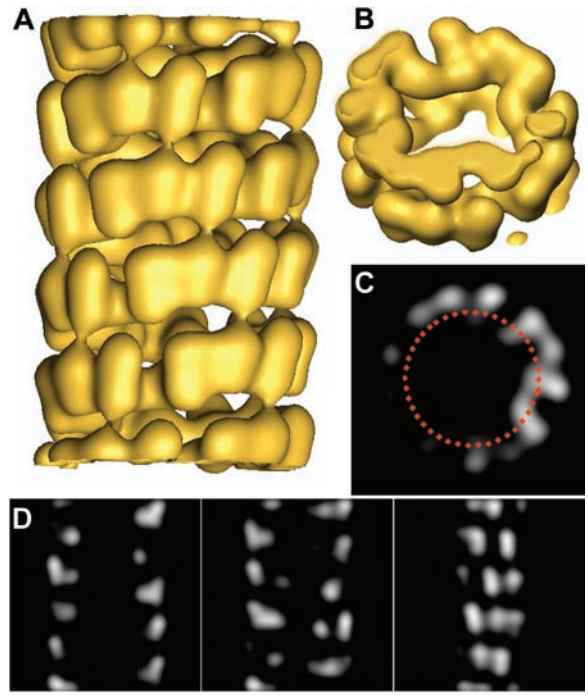

FIG. 2. *A*, a three-dimensional reconstruction of the VirE2-ssDNA complex. The outer diameter of the helix is 15.7 nm, and its inner diameter is 7.0 nm. The isosurface is viewed from outside. The isosurface threshold is estimated to contain 100% of the mass of enclosed protein and DNA. *B*, tilting and shortening the isosurface representation provides a view of the interior of the solenoidal complex. The shelf-like protrusion matches the internal ledge apparent in the averaged image shown in the *rightmost panel* of Fig. 1*B*. *C*, a volume density representation is shown in a slice perpendicular to the helical axis. The *red ring* has a diameter of 11 nm, representing the estimated location of the ssDNA. *D*, slices through the volume density are shown in slices parallel to the helical axis (through the center, near the inner surface, and near the outer surface).

tal Procedures" (Fig. 1*B*). The particles were low pass-filtered to 2.5 nm, their phases were corrected for CTF, and a reference-free alignment was carried out (aligned average shown in *rightmost panel* of Fig. 1*B*). The pitch can be measured directly at ~5.2 nm. The same value was obtained from Fourier transforms of individual long filaments selected from the micrographs, suggesting a strong regularity. The filament also appears to be polar with a hooked ledge between the outer surface and a hollow interior.

A three-dimensional reconstruction was produced from the CTF-corrected data set using the IHRSR method (42). Helical symmetry was found with an angle between successive subunits of roughly 85°, corresponding to 4.25 ± 0.05 subunits/helical turn and a pitch of 5.15 ± 0.02 nm, in agreement with the two-dimensional average. The isosurface is shown in Fig. 2*A*, with the threshold chosen to enclose 100% of the estimated mass of protein and ssDNA. Note that the hooked ledge appears as an inwardly protruding shelf on the isosurface, as is apparent in the tilted view of Fig. 2*B*. Fig. 2, *C* and *D*, shows slices of reconstructed density in a cut normal to the helical axis (*C*) and in three planes parallel to it (*D*). The outer surface is quite open, with a deep cleft suggesting a site for tight interaction with other bacterial or plant proteins. The most interesting feature is on the inner surface, where a protrusion appears forming a nearly continuous shelf around the inner perimeter. The diameter of the complex at the innermost surface is 7 nm.

The handedness of the three-dimensional reconstructed T-complex was determined by imaging tilted specimens following the method of Finch (47). We found the solenoid to be right-handed.

To try to localize the DNA, we estimated the average radius at which the DNA sits. The length of the M13 ssDNA substrate is 7249 bases and has a mass of 2392 kDa. Assuming a canonical extended length of 0.4 nm/base for single-stranded DNA, this implies a total length of 2900 nm. The mass of VirE2, calculated from the amino acid sequence, is 63.4 kDa. Nitrocellulose binding assays indicated a stoichiometry of 10:1 protein:DNA by weight for complete coverage (22). We confirmed this figure by electrophoretic gel retardation (data not shown). The number of VirE2 proteins/M13 DNA molecule is then 23920/63.4 = 377. At 4.25 VirE2/turn, this would indicate 88 complete helical rings. The length of ssDNA/ring is thus 32.6 nm, or 82 bases, implying a binding of ~19 nucleotide bases/protein. The average diameter of the DNA within the helix is then estimated at 10.5 nm. An alternate estimate may be made by measuring the length around the perimeter of well formed circular complexes. This yielded an average of 425 nm, *i.e.* a 7-fold reduction of the original oligonucleotide length. With a pitch of 5.2 nm, this implies ~35 nm of extended ssDNA/ring, yielding an average diameter of 11 nm. The good agreement between these estimates confirms the determination of binding stoichiometry. A colored ring at 11-nm diameter is depicted on the density plot in Fig. 2*C*.

In addition to the solenoidal structure, VirE2 also forms aggregates even in the absence of DNA. Early biochemical evidence suggested that these are probably tetramers (21), while recent evidence points to trimers.[2] In the presence of ssDNA, ring-like objects also appeared on the grids. They were often found next to the ends of helical filaments, where the circular DNA had broken to linear segments (Fig. 3*A*). A two-dimensional alignment and an average of such objects confirmed that they are in fact tetrameric rings (Fig. 3, *B* and *C*). Note that these rings appear even though ssDNA is in excess with respect to saturated binding of the protein.

To verify the match between the two-dimensional average of the tetrameric rings and the three-dimensional reconstruction, the former was overlaid onto a slice through the latter, which was cut at an angle slightly tilted from normal to the helical

[2] A. Engel, personal communication.

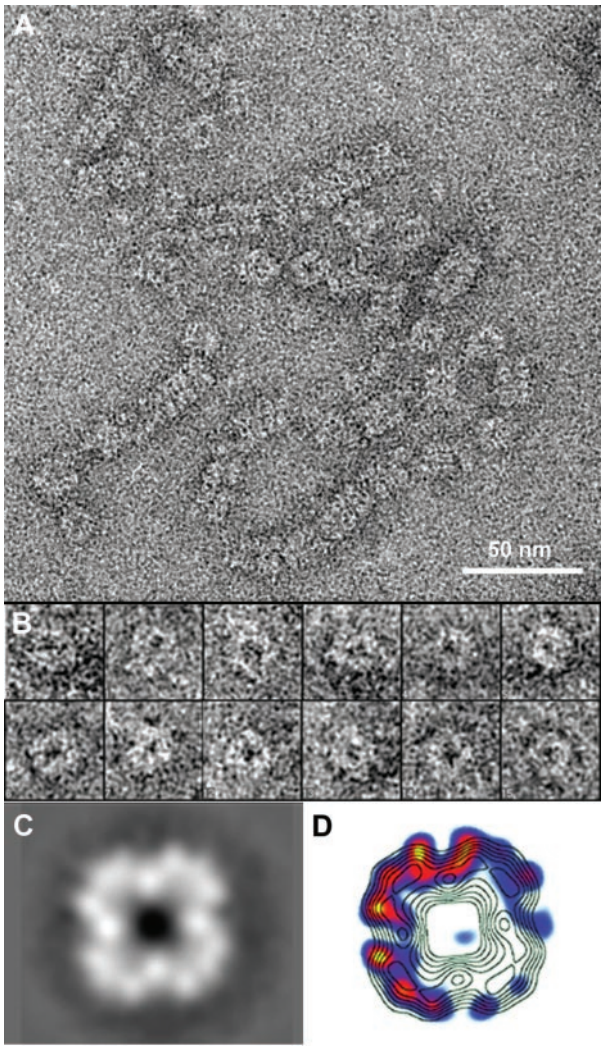

FIG. 3. *A*, a raw image of ring-like structures interspersed with the helical assemblies. *B*, a gallery of selected ring-like particles. *C*, a two-dimensional average of rotationally and translationally aligned rings shows clear 4-fold rotational symmetry. Symmetry is not imposed in this image. *D*, isocontour lines from a C4-symmetrized version of the image in *C* are shown overlaid onto a slice through the three-dimensional reconstruction. Note the good agreement in the major features of the two independent analyses.

axis so as to optimize the overlap. A contour representation of the two-dimensional average is shown on top of a false color density map of the slice in Fig. 3*D*. Although the fit cannot be perfect all the way around the circle, due to incommensurate matching, it is clear that the individual protein units match in a very satisfactory way.

DISCUSSION

The complex of single-stranded DNA with VirE2 protein forms a right-handed solenoidal structure as depicted in Fig. 2. Based on geometric considerations we can place the oligonucleotide at an average radius of ~11 nm, close to the inner face of the protein. We also observe an alternate organization of the VirE2, as tetramers. These tended to lie nearby the ends of helices formed at breaks in the circular ssDNA substrates. The rings are likely to contain ssDNA because DNA is still in large excess in our experimental conditions, and there is high affinity for VirE2-DNA binding. This alternate quaternary organization of the protein provides an independent means to verify the three-dimensional reconstruction. Note that the two data sets were produced independently and represent views of orthogonal projections, along the central axis for the tetramers and normal to it for the solenoid. Protrusions appearing on the isosurface also appear in the tetramer average so that the shapes of the protein units are quite similar. There is some discrepancy in the depth of the indentations on the reconstruction. These appear to interrupt the shelf along the inner surface and to suggest a deep cleft at the outer surface. Such indentations also appear in the tetramer average but with smaller amplitude in the isocontour lines. This discrepancy may be due in part to differences in staining. In the case of the tetramers the interior surface is clearly more accessible than in the closed solenoids.

Individual protein units comprise two major domains facing outward and an inward facing linker domain. One of the outward facing domains splits to two subdomains, giving the appearance of three outward pointing lobes. Approximate dimensions of the protein (as seen on the isosurface representation, Fig. 2, *A* and *B*) are 5.2 nm in height, 4.3 nm radially, and 8.1 nm circumferentially, evaluated at the putative DNA-binding radius of 5.5 nm.

A previous study of VirE2-ssDNA by scanning transmission electron microscopy originally proposed the solenoidal (telephone coil) structure (40), although without molecular resolution. That work reported a outer diameter of 12.6 nm for the complex, using the criterion of full-width at half-maximum density in the scanning transmission electron microscopy imaging. As expected, this is slightly smaller than the full extent of the isosurface shown here. On the basis of mass measurements it was estimated that there should be 3.4 VirE2 proteins/helical turn. The tetramer form gave us confidence, on the other hand, in assigning roughly 4 units/turn, and the dimensions observed for the protein units themselves are internally consistent between the two-dimensional average and the three-dimensional reconstruction. From the latter we can also estimate the mass/length. Over the pitch of 5.2 nm we have 4.25 VirE2 proteins and 82 DNA bases, for a mass of 270 + 26 kDa = 296 kDa, or 57 kDa/nm, essentially identical to the prior scanning transmission electron microscopy measurement of 58 kDa/nm (40).

Our reconstruction of the VirE2-ssDNA complex brings some insight into the advantages of ssDNA association with VirE2. First, the structure shows how the ssDNA may be protected from attack by cytoplasmic nucleases (48), as it is sequestered within the interior of the protein cylinder. Secondly, the DNA is compressed into a compact form. Whereas pathogenic tDNA is roughly 20 kb in length, successful transformation may be achieved with tDNA as long as 150 kb. These correspond to extended physical lengths of 8 and 68 microns, respectively. Association with VirE2 reduces these by about 7-fold to more reasonable subcellular dimensions. The T-complex would also prevent alternative DNA secondary structures that might tend to form with such a long polymeric molecule. Such structures, or even a random coil of uncontrolled shape, would have difficulty moving through the cytoplasm. Third, the structure shows how VirE2 monomers are readily available for binding to cofactors. Recently it was shown that VirE2 associates with the plant nuclear import receptor karyopherin α in *Arabidopsis thaliana* via an obligatory interaction with the plant-specific host cell factor VIP1. For this reason it is apparently inactive in animal cells, while co-transfection of VirE2 with VIP1 in yeast and mammalian cells leads to its nuclear localization (33). Thus it is reasonable to assume that the VirE2-ssDNA complex that we observe *in vitro* is further decorated *in vivo* by VIP1 and karyopherin α, where the latter mediates passage of the entire assembly through the nuclear pore. Indications from animal systems suggest that the nuclear pore can accommodate substrates of diameters exceeding 26 nm (49), or even as

large as 39 nm (50), when associated with appropriate karyopherin (importin) transport receptor proteins. Thus the outer diameter of 16 nm is small enough, even with such a decoration, that translocation through the nuclear pore would not require unwinding or any other disassembly of the complex. Note that the DNA is entirely hidden from host factor interactions with the VirE2, consistent with the lack of specific sequence requirements for its nuclear import.

Transfer DNA from *Agrobacterium* is always in linear form. The coexistence of flat tetramers with the extended solenoidal form suggests a means of nucleating the latter, as well as the tendency to make kinks or other breaks in the regular helical phase. Four monomers may close into a ring when bound to DNA, but a slip in the closure would permit continuation around a growing spiral. Should the spiral close at some point, another nucleation occurring along the dangling length of the bare DNA would not be in phase with the first, leaving a break or kink in the overall structure. It is interesting to speculate whether such kinks may have a biological function, perhaps one as simple as allowing the T-complex to fold at intervals. The symmetrized volume shown in Fig. 2 may give an exaggerated impression as to the regularity of the VirE2-ssDNA complex. In practice, typical distances between obvious breaks were observed in the range of 30–100 nm and depended rather sensitively on details of sample preparation. We can suggest that the solenoid forms in delicate balance between the tendency of the protein to associate with itself in a planar configuration and its affinity to binding ssDNA in a continuous manner. Under our experimental conditions, the latter must be preferential since we do see predominantly extended spirals. Precedence for alternate ring-like or helical binding to ssDNA is found in the case of archaeal RadA protein (51).

Geometric considerations place the ssDNA inside the protein spiral formed by the VirE2-ssDNA complex, suggesting the importance of the internal shelf-like domain that is observed. Further studies at a higher resolution using cryopreparation methods will be required to model the DNA specifically and to elucidate its interaction with particular protein motifs. Looking to the outside of the protein, this work should serve as a basis for decoration studies with VIP1 and other factors involved in T-complex nuclear import.

Acknowledgments—We thank Andreas Engel for comments and discussions and Shachar Oliel for assistance with protein expression. Advice from Ed Egelman and Bernard Heymann on image processing is gratefully acknowledged.

REFERENCES

1. de Cleene, M., and de Ley, J. (1976) *Bot. Rev.* **42,** 389–466
2. Escobar, M. A., and Dandekar, A. M. (2003) *Trends Plant Sci.* **8,** 380–386
3. Gelvin, S. B. (2000) *Annu. Rev. Plant Physiol. Plant Mol. Biol.* **51,** 223–256
4. Gelvin, S. B. (2003) *Microbiol. Mol. Biol. Rev.* **67,** 16–37
5. Zupan, J., Muth, T. R., Draper, O., and Zambryski, P. C. (2000) *Plant J.* **23,** 11–28
6. Tzfira, T., and Citovsky, V. (2000) *Mol. Plant Pathol.* **1,** 201–212
7. Tzfira, T., and Citovsky, V. (2002) *Trends Cell Biol.* **12,** 121–129
8. Gaudin, V., Vrain, T., and Jouanin, L. (1994) *Plant Physiol. Biochem.* **32,** 11–29
9. Ishida, Y., Saito, H., Ohta, S., Hiei, Y., Komari, T., and Kumashiro, T. (1996) *Nat. Biotechnol.* **14,** 745–750
10. Piers, K. L., Heath, J. D., Liang, X., Stephens, K. M., and Nester, E. W. (1996) *Proc. Natl. Acad. Sci. U. S. A.* **93,** 1613–1618
11. de Groot, M. J., Bundock, P., Hooykaas, P. J., and Beijersbergen, A. G. (1998) *Nat. Biotechnol.* **16,** 839–842
12. Gouka, R. J., Gerk, C., Hooykaas, P. J., Bundock, P., Musters, W., Verrips, C. T., and de Groot, M. J. (1999) *Nat. Biotechnol.* **17,** 598–601
13. Kunik, T., Tzfira, T., Kapulnik, Y., Gafni, Y., Dingwall, C., and Citovsky, V. (2001) *Proc. Natl. Acad. Sci. U. S. A.* **98,** 1871–1876
14. Peralta, E. G., and Ream, L. W. (1985) *Proc. Natl. Acad. Sci. U. S. A.* **82,** 5112–5116
15. Wang, K., Stachel, S. E., Timmerman, B., Van Montagu, M., and Zambryski, P. C. (1987) *Science* **235,** 587–591
16. Sheng, J., and Citovsky, V. (1996) *Plant Cell* **8,** 1699–1710
17. Valentine, L. (2003) *Plant Physiol.* **133,** 948–955
18. Gelvin, S. (2003) *Trends Biotechnol.* **21,** 95–98
19. Young, C., and Nester, E. W. (1988) *J. Bacteriol.* **170,** 3367–3374
20. Durrenberger, F., Crameri, A., Hohn, B., and Koukolikova-Nicola, Z. (1989) *Proc. Natl. Acad. Sci. U. S. A.* **86,** 9154–9158
21. Sen, P., Pazour, G. J., Anderson, D., and Das, A. (1989) *J. Bacteriol.* **171,** 2573–2580
22. Citovsky, V., Wong, M. L., and Zambryski, P. C. (1989) *Proc. Natl. Acad. Sci. U. S. A.* **86,** 1193–1197
23. Christie, P. J., Ward, J. E., Winans, S. C., and Nester, E. W. (1988) *J. Bacteriol.* **170,** 2659–2667
24. Gelvin, S. B. (1998) *J. Bacteriol.* **180,** 4300–4302
25. Citovsky, V., Zupan, J., Warnick, D., and Zambryski, P. C. (1992) *Science* **256,** 1802–1805
26. Vergunst, A. C., Schrammeijer, B., den Dulk-Ras, A., de Vlaam, C. M. T., Regensburg-Tuink, T. J., and Hooykaas, P. J. J. (2000) *Science* **290,** 979–982
27. Zupan, J., Ward, D., and Zambryski, P. C. (1998) *Curr. Opin. Microbiol.* **1,** 649–655
28. Ballas, N., and Citovsky, V. (1997) *Proc. Natl. Acad. Sci. U. S. A.* **94,** 10723–10728
29. Scheiffele, P., Pansegrau, W., and Lanka, E. (1995) *J. Biol. Chem.* **270,** 1269–1276
30. Relic, B., Andjelkovic, M., Rossi, L., Nagamine, Y., and Hohn, B. (1998) *Proc. Natl. Acad. Sci. U. S. A.* **95,** 9105–9110
31. Mysore, K. S., Bassuner, B., Deng, X. B., Darbinian, N. S., Motchoulski, A., Ream, L. W., and Gelvin, S. B. (1998) *Mol. Plant-Microbe Interact.* **11,** 668–683
32. Bako, L., Umeda, M., Tiburcio, A. F., Schell, J., and Koncz, C. (2003) *Proc. Natl. Acad. Sci. U. S. A.* **100,** 10108–10113
33. Tzfira, T., Vaidya, M., and Citovsky, V. (2001) *EMBO J.* **20,** 3596–3607
34. Ziemienowicz, A., Merkle, T., Schoumacher, F., Hohn, B., and Rossi, L. (2001) *Plant Cell* **13,** 369–384
35. Zupan, J., Citovsky, V., and Zambryski, P. C. (1996) *Proc. Natl. Acad. Sci. U. S. A.* **93,** 2392–2397
36. Dumas, F., Duckely, M., Pelczar, P., Van Gelder, P., and Hohn, B. (2001) *Proc. Natl. Acad. Sci. U. S. A.* **98,** 485–490
37. Duckely, M., and Hohn, B. (2003) *FEMS Microbiol. Lett.* **223,** 1–6
38. Frary, A., and Hamilton, C. M. (2001) *Transgenic Res.* **10,** 121–132
39. Hamilton, C. M. (1997) *Gene* (*Amst.*) **200,** 107–116
40. Citovsky, V., Guralnick, B., Simon, M. N., and Wall, J. S. (1997) *J. Mol. Biol.* **271,** 718–727
41. Heymann, J. B. (2001) *J. Struct. Biol.* **133,** 156–169
42. Egelman, E. H. (2000) *Ultramicroscopy* **85,** 225–234
43. Marabini, R., Masegosa, I. M., San Martin, M. C., Marco, S., Fernandez, J. J., de la Fraga, L. G., Vaquerizo, C., and Carazo, J. M. (1996) *J. Struct. Biol.* **116,** 237–240
44. Frank, J., Radermacher, M., Penczek, P., Zhu, J., Li, Y., Ladjadj, M., and Leith, A. (1996) *J. Struct. Biol.* **116,** 190–199
45. Ludtke, S. J., Baldwin, P. R., and Chiu, W. (1999) *J. Struct. Biol.* **128,** 82–97
46. Owen, C. H., Morgan, D. G., and DeRosier, D. J. (1996) *J. Struct. Biol.* **116,** 167–175
47. Finch, J. T. (1972) *J. Mol. Biol.* **66,** 291–294
48. Ward, D. V., and Zambryski, P. C. (2001) *Proc. Natl. Acad. Sci. U. S. A.* **98,** 385–386
49. Feldherr, C. M., and Akin, D. (1990) *Electron Microsc. Rev.* **3,** 73–86
50. Pante, N., and Kann, M. (2002) *Mol. Biol. Cell* **13,** 425–434
51. Yang, S., Yu, X., Seitz, E. M., Kowalczykowski, S. C., and Egelman, E. H. (2001) *J. Mol. Biol.* **314,** 1077–1085